Multi-instrumented analysis of fatigue behavior and damage mechanisms in jute fiber-reinforced polyester composites

Adem Alia, Gilbert Fantozzi, Nathalie Godin, Jérôme Adrien, Hocine Osmani, Pascal Reynaud

Multi-instrumented analysis of fatigue behavior and damage mechanisms in jute fiber-reinforced polyester composites

Adem Alia[a,b], Gilbert Fantozzi[a], Nathalie Godin[a], Jérôme Adrien[a], Hocine Osmani[b], Pascal Reynaud[a]
[a] University of Lyon, INSA-Lyon, MATEIS UMR CNRS 5510, Bat. Blaise Pascal, 7 avenue Jean Capelle, 69621 Villeurbanne, France
[b] University of Sétif 1, IOMP, LMNM, Avenue Said Boukhrissa, 19000 Sétif, Algeria

Abstract

The present work deals with the fatigue behavior of a jute fiber-reinforced polyester composites. Two stacking sequences were considered $[0]_8$ (JP_0) and $[+45/-45]_{2S}$ (JP_45). The fatigue lifetimes diagrams were determined. They exhibit a fatigue limit lower than 20 MPa for JP_0 composites and lower than 15 MPa for JP_45, whereas the mean ultimate tensile stress σ_R is 42.9 MPa for JP_0 and 31.1 MPa for JP_45, and the lifetimes lower than 500 000 cycles for JP_0 and 250 000 cycles for JP_45. An exhaustive analysis of the fatigue damage is carried out by combining four approaches: measurement of the mechanical parameters, microscopic observations, X-ray tomography, acoustic emission (AE) monitoring. X-ray tomography revealed the presence of multiple fiber/matrix debondings within transverse yarns for the composites $[0]_8$ and yarn/matrix debondings for the composites $[+45/-45]_{2S}$. Density of matrix cracks is always more important (about 80%) for JP_45 than for JP_0 at the same relative stress level/σ_R, and decrease of a 3 times factor for JP_0 (5 for JP_45) when the relative stress increases from 50% to 80%. Two types of behaviors are observed: one for low stresses and another for high stresses. Damage evolution is followed by AE by using a supervised classification with 3 classes of events: matrix cracking, fiber/matrix debonding and fiber breakage. The global activities are at the most of 600 000 signals, and decreases 10 times from 50% σ_R to 80% σ_R. The results of AE highlighted in addition the greater number of matrix cracks for low stresses in agreement with X-ray tomography in the same proportions. High stresses are characterized by a larger number of fiber breaks (4 times for both composites) and fibre/matrix debondings (2 times) for JP_0, unless for fiber/matrix debonding in JP_45 which decreases 3 times. The multi-instrumented damage approach allows to make a precise and quantitative analysis of the fatigue damage mechanisms. The results highlight that for the weak stress levels matrix cracking is predominating whereas for the high stress levels the fiber breakages are significant. A scenario of fatigue damage is

proposed: for low stresses the behavior is controlled by the matrix and for high stresses the behavior is controlled by the fibers.

Keywords: Fatigue, jute fiber, polyester matrix composite, multi-instrumentation, acoustic emission, damage mechanisms, X-Ray tomography

1. Introduction

The mechanical behavior of natural plant fiber reinforced polymer composites (NFRP) is broadly studied in the literature and the majority of the papers concerned the mechanical behavior of NFRPs reinforced with flax or hemp fibers [1-4]. Some papers deal more specifically with the mechanical characterization under monotonic tension of polymer composites reinforced with jute fibers and polyester matrix [5-7], and show that their mechanical resistances are comparable. In the previous study [6] on the jute/polyester composite of the present paper, the mechanical properties are also similar than from the other composites of the literature, but the damage scenario is more precise and detailed.

Regarding the fatigue behavior, most of the papers concerning the NFRPs deal with flax fibers and few deal with jute/polyester composites [12]. Recently Mahboob and Bougherara [9] have written a significant review concerning the fatigue behavior of flax-epoxy and other NFRPs. The general characteristics concerning the fatigue of NFRPs are reviewed. Firstly, the fatigue damage mechanisms observed by following strength and stiffness degradation of NFRPs seem similar regardless of the plant type for composites reinforced with flax, hemp and jute fibers [12, 17, 18, 19]. The mechanical parameters as stiffness, residual or mean strain follow a 3-stages evolution with the first and third stages with a more rapid variation and the second stage with a lower degradation rate [8, 10]. Fatigue damage modes in NFRPs are similar to those observed during monotonic loading: matrix cracking, fiber-matrix debonding, fiber breakage and pull-out, delamination [11, 13]. These damage mechanisms can be identified by using different techniques such as digital image correlation (DIC), X-ray computed tomography (CT), microscopic observations or acoustic emission (AE) [14, 15, 10, 20]. The evolution of damage mechanisms can be described by a three stages scenario: the first one corresponds to transverse matrix cracking and interface damage with some weak fiber breakages, the second one deals with the development of matrix cracking, significantly along interfaces and in the third stage, macroscopic matrix cracks and interface damage develop, and yarn failures occur. It can be noticed that fiber failures appear early and later during the fatigue life of [0°/90°] composites and are rarely observed for the [+45°/-45°]

composites. The papers studying the fatigue behavior of the NFRPs using AE technique are essentially focused on one temporal parameter (amplitude) in order to define damage modes. Some researchers [18,19] consider both temporal and frequential features of the AE signals to perform a more efficient analysis of AE.

There is a lack of researches on fatigue behavior of jute fiber-reinforced polymer composites, and the aim of this paper is to investigate this specific composite. Our multi-instrumented approach takes into account the most relevant methodologies developed in the literature, in order to better analyze and quantify the damage evolutions during fatigue. Recently, we have studied the static mechanical behavior of jute fiber-reinforced polyester composite and characterized the damage mechanisms using AE and microstructural observations [6]. The damage mechanisms were observed using microscopic observations (SEM) and X-ray computed tomography: fiber-matrix debonding which is the more significant damage, matrix cracking and fiber breakage.

Hence, it is interesting to study the fatigue behavior of the same woven jute fiber-reinforced polyester composite used for the monotonic loading [6] and to specify the damage modes observed during cyclic fatigue loading of this particular composite, compared to the other NFRP composites of the literature. It is the objective of the present paper. In order to make a precise and quantitative analysis of fatigue damage mechanisms, a multi-instrumented approach is used by combining different techniques: macroscopic mechanical parameters evolutions, acoustic emission monitoring, microstructural observations, X-ray tomography.

2. Materials and methods

2. 1. Fabrication of laminates

The jute fibers reinforced polyester (JFRP) composites have already been used in [6]. As for the previous study, the plates were made from 8 balanced taffetas jute fabrics supplied by Complexe de jute (Bejaia, Algeria) and from unsaturated polyester resin marketed by Maghreb Pipe (M'sila, Algeria). All fabrics were used as received (without any treatment). They are constituted of untwisted weft and warp yarns and have a density of 1460 +/-20 kg/m^3. The JFRP plates with a dimension of 300×200×8 mm^3 were manufactured using a hand lay-up composites fabrication technique. The fabrics were dried in an oven at 110°C to remove adsorbed water before being stacked on top of each other inside a mold. Then the polyester resin was added to impregnate them, and to optimize the resin polymerization

(jellification and hardening) the laminates were cured 24 h at room temperature under pressure inside the mold, prior to resting in air for 10 days [27]. Finally, composites are heated some hours at 110°C to finish the reticulation of the resin.

Due to jute fabrics characteristics, resulting composites plates were characterized by a fiber volume fraction of 28 ± 2% (measured by the Archimede's method) and a void content of about 2 %. As in the previous work [6], two stacking sequences were considered: the first one, referred as $[0]_8$ (noted JP_0), the second one, referred as $[+45/-45]_{2S}$ (noted JP_45). These two stacking sequences were chosen to obtain symmetric composites with intermediate thicknesses allowing a better observation of plies in the core of the composites, and the two orientations (0°/90) and (+/-45°) leading to a better mechanical characterization of strong and weak (more subjected to shear) directions of this composite. For the JP_0 composites, tests were conducted on dumbbell specimens so that the breakage would occur in the gauge length. For the JP_45 composites, rectangular specimens were cut (without lubrication) from obtained laminate plates with dimensions of 160 ×15 ×8 mm^3.

2.2. Tension-tension fatigue tests

In this study, mechanical tests were mainly performed under fatigue following the recommendations of the standard NF EN ISO 17140. They were performed on an hydraulic uniaxial testing machine (MTS 810 with a load cell capacity of 100 kN) fitted with hydraulic grips for the specimen fixation, and instrumented with a 2 knifes extensometer (gauge length of 25 mm) and 2 acoustic emission (AE) sensors (Fig.1). The extensometer is placed on the face of the specimen. In this configuration, the direct measurement of the strain is representative of the first layer of the composite. Nevertheless, during all the mechanical tests, no delamination has been observed and the fracture strain is low (1.2% +/-0.2%), hence the strain measured may be assumed to be representative of the deformation of the whole composite even of the plies inside the composite and not only of the superficial plies. According to the low level of deformation of these composites, the tensile stresses are calculated by the ratio of the load applied over the initial cross section of the specimens.

In order to investigate the fundamental fatigue behavior of this composite, all tests were carried out at room temperature under load amplitude control mode with a constant stress ratio $R = \sigma_{min}/\sigma_{max} = 0.01$ (to stay in tensile/tensile conditions and have experimental conditions leading to the most developed stress/strain loops in this stress domain) and a constant frequency f = 1 Hz (to allow stress/strain recording in good experimental conditions),

and four levels of maximum stresses corresponding respectively to 50%, 60%, 70% and 80% of the ultimate tensile stress σ_R (42.9 MPa for JP_0 and 31.1 MPa for JP_45 [6]) were tested for the two layups. These tests were run at a stress level higher than the fatigue limit (about 40% σ_R) hence conducted up to the fracture and full separation of the composite, where the lifetime was lower than 5.10^5 cycles. At least four replicates were tested at each stress level. More details on the mechanical characteristics under monotonic loading up to fracture and full separation of these composites, and ultimate tensile stresses determination are given in a previous paper [6].

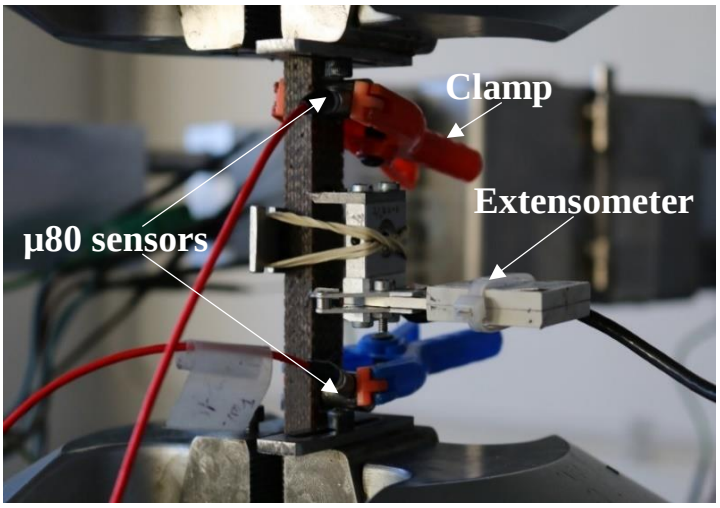

Fig. 1. Experimental device with extensometer and AE sensors fixed on a tensile specimen

During the fatigue tests, the stress-strain loops were recorded with a pseudo logarithmic sequence (all cycles up to 1000, then one cycle each 10 cycles up to 10 000 cycles, one cycle each 100 cycles up to 100 000 cycles, …). For each cycle recorded, stress and strain are recorded in relationships with time, allowing to follow the evolution of the stress/strain loops. To quantify these evolutions, several mechanical parameters might be determined, and among them three are particularly followed in the present study (see Fig. 2): the dynamic secant modulus Es (corresponding to the slope of each stress/strain loop: $E_s = (\sigma_{max}-\sigma_{min})/(\varepsilon_{max}-\varepsilon_{res})$), the minimum (or residual) strain ε_{Res} (strain at σ_{min}), and the internal friction. The latter is the ratio between the dissipated energy (area of the stress/strain loop called ΔW) and the maximum elastic energy stored during a cycle (W) (yellow portion in Fig. 2). They have been calculated for each recorded loops and plotted in relationships with the number of applied cycles.

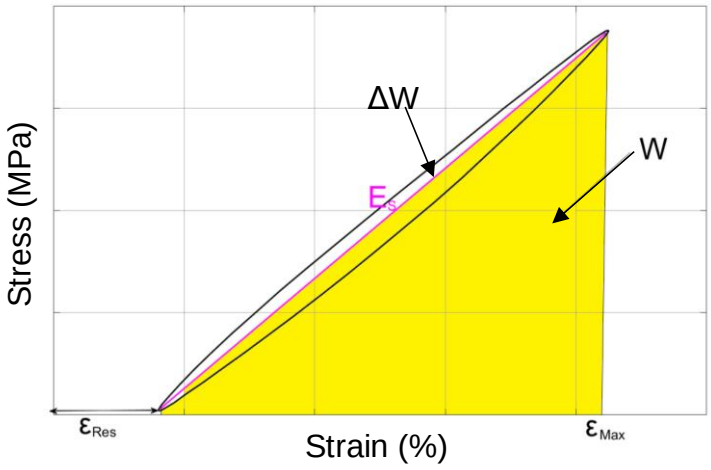

Fig. 2. Stress-strain hysteresis loop and mechanical parameters measured during the fatigue cycles.

2.3. Microscopic observations

In order to assess the damage mechanisms for the different stress levels, fractured surfaces were examined using a Zeiss Supra scanning electronic microscope (SEM) for the two layups. Polished lateral sections extracted from the broken samples were also examined using electronic and optical microscopies.

2.4. X-ray computed tomography

X-ray computed tomography observations were conducted by using a laboratory v/Tome/X tomograph (Phoenix, Germany). A 10 µm resolution has been used in this work with an accelerating voltage of 80 kV and a beam current of 280 µA. In order to realize a detailed analysis of the damage occurrence and to compare the cracks density for the different stress levels, all observed samples with the same dimension were cut close to the breakage zone. The image acquisition time was about 1 h per specimen. The 3D reconstruction was obtained by a standard filtered back projection algorithm implemented in the software coupled to the tomography.

2.5. Acoustic emission

AE monitoring was achieved continuously during the fatigue tests using a classic MISTRAS PCI 2 data recording system with AEWIN software, with the same configuration than the one used for the monotonic tensile tests described in the paper [6], where more

technical details are given. The AE signals were recorded using two resonant Micro-80 piezoelectric sensors. They were placed at the gauge extremities, with a distance of 70 mm between their centers in order to locate the AE events.

A supervised classification technique is used to investigate AE signals recorded during fatigue tests and the damage mechanisms as shown recently for flax fibers reinforced epoxy composites [26]. This technique requires a data base of labelled signals: the training set. This one is created by merging data collected during tensile tests on the two stacking sequences. As described in a previous paper [6], the AE data were processed using an unsupervised pattern recognition technique combining principal component analysis and k-means optimized by a genetic algorithm. This analysis of AE signals led to the identification of 3 types of AE signals and to the following labelling of classes [6]:

- Class 1, contains signals of low frequency (250 kHz) and intermediate amplitude (about 55 dB),
- Class 2, characterized by signals of higher frequency (420 kHz) and similar amplitude than Class 1 (about 60 dB)
- Class 3 which contains the signals of higher amplitude (about 78 dB) and intermediate frequency (400 kHz).

Signals of class 2 appear first, then those of class 1 and finally class 3. By making interrupted tensile tests, SEM observations and X-ray tomography, the signals of class 2 were attributed to the fiber-matrix debondings, those of class 1 to matrix cracking and class 3 was assigned to fiber breakage and pull-out. So, AE allows to describe the kinetics of evolution of each damage mode of the composite.

In order to establish the training set of labelled signals for the supervised analysis, the same number of signals (800 signals) of each class is used. For fatigue tests, on this kind of materials, it is not necessary to introduce an additional class which includes friction, sliding at fiber/matrix interfaces and closing of matrix cracks. Indeed, during these tests, AE signals are only recorded during the loading part of the cycle. So, this training set includes all the damage mechanisms that may operate in this composite during fatigue. The supervised classification is based on a random forest algorithm, software denoted RF-CAM ("Random Forests Classification for Acoustic emission Monitoring"). Details of this algorithm are not given here for the sake of brevity. Readers should refer to the cited reference [22, 23]. The main assumption for a supervised classification is that labels of learning signals are true. But

certainly, in the dataset, some learning data have wrong labels. Morizet et al. [23] with artificial datasets illustrating the problem of supervised classification under uncertainty shows that the Random Forest algorithm is little sensitive to a slightly mislabeled library, in fact the recognition results are satisfactory even if classes are altered up to 20%. Each signal is described by 26 descriptors, calculated in time and frequency domains (Amplitude, duration, peak frequency…). Using signals of the learning library, 200 decision trees has been trained. During the testing phase, each AE signal runs down each tree of the forest, leading to T votes. The final decision is obtained by the security voting rule. In this case, a given AE signal is assigned to a specific class if more than 70% of the total number of trees voted for that class. For the fatigue tests, between 79% and 92% of the classified signals validate this rule. As shown in section 3.5, the acoustic activity is rather high during fatigue tests (which durations are up to 100h), but the number of localized signals (lower then 60 000) may be easily numerically analyzed and correspond to several signals per cycle.

3. Results and discussion

3.1. S-N curves

Fatigue tests were conducted on the two layups (JP_0 and JP_45). Four tests were conducted per stress level. The average numbers of fatigue cycles until failure (N_f) with the standard deviation between brackets are summarized in Table 1.

Table 1

Mean lifetimes N_f and standard deviation of jute/polyester composites subjected to cyclic fatigue (R = 0.01, f = 1 Hz).

	50% σ_R	60 % σ_R	70 %σ_R	80 % σ_R
N_f (JP_0)	263 527 +/- 128 856	48 863 +/- 26 732	24 294 +/- 9 570	4 292 +/- 1 530
N_f (JP_45)	172 591 +/- 84 442	30 852 +/- 4 554	4 877 +/- 1 118	1 079 +/- 310

To analyze fatigue S–N curve results, an empirical power-law based model developed by D'Amore et al. [21] was used to fit the S-N curves. The interest of this model is to consider the nonlinear effect of the stress ratio on the fatigue live. This model was initially developed and verified for random glass–fiber-reinforced plastics with thermosetting resin. It was used after that by de Vasconcelos et al. [10] to analyze fatigue results obtained in tension-tension

solicitation of woven hemp fiber reinforced epoxy composite and the results showed a good accordance between experimental data and the model. The model is given as follows [21]:

$$N_f = \left[1 + \frac{1}{a(1-R)}\left(\frac{\sigma_R}{\sigma_{max}} - 1\right)\right]^{\frac{1}{b}}$$

where σ_R is the static tensile strength, σ_{max} is the maximum stress during fatigue cycling, R is the stress ratio, a and b are two material parameters to be experimentally determined. In the present work, the ultimate tensile stresses σ_R used are issued from monotonic tensile tests described in a previous paper [6].

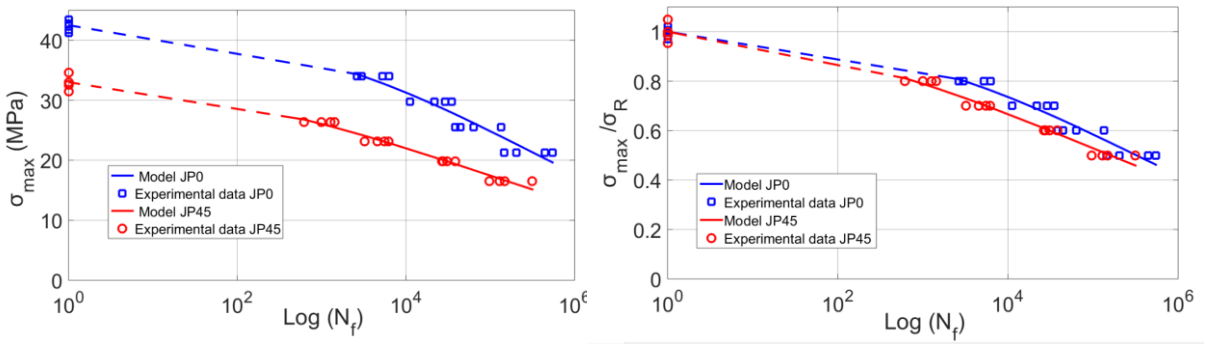

Fig. 3. Fatigue lifetimes diagrams (S-N curves): experimental data and D'Amore modeling for the two lay-ups: a) σ_{max} as a function of log (N_f), b) normalized stress as a function of log (N_f) (the coefficient of correlation R^2 =0.945 and 0.982 for JP_0 and JP_45 composites respectively).

Fig. 3 presents the S-N curves for the fatigue tests results, where the maximum fatigue stress is plotted versus the logarithm of the number N_f of cycles to failure (showed by the colored circles). All samples failed during fatigue tests even for low stress levels and for the two laminates. It can be noticed that for the two studied layups, the number of cycles to failure decreases gradually when increasing the fatigue stress level, with some scattering in the fatigue lifetime for a given stress level. The D'Amore model represented by the solid lines in Fig. 3 fits correctly the experimental data (coefficient correlation, R^2 =0.945 for JP_0, and R^2 = 0.982 for JP_45). The parameters a and b were determined by a mean-square calculation under a constant R, no cumulated fatigue is considered here. For each stacking sequences a and b are equal respectively to 0.0244 and 0.3074 for JP_0 laminates, and to 0.0706 and 0.2277 for JP_45 ones. It can be noticed that the JP_0 composites exhibit a steeper decrease in

fatigue strength as a function of fatigue cycles to failure, mainly described by the variation of the parameter b.

3.2. Evolution of the mechanical parameters

The evolution of aforementioned mechanical parameters as a function of the normalized fatigue cycles N/N_f and for the two layups are presented in Fig. 3a-f. The evolution of these parameters is an interesting indication of the damage evolution. The presented curves correspond to the mean values of the measured data for the four tests and for each stress level. The scattering bars represent the dispersion of data for a given stress level. Figures below show the hysteresis loop recorded during the fatigue tests for the lower and higher stress levels and for the two composites (JP_0 and JP_45). Loops at N=1, N=0.25 N_f, N=0.75 N_f and N=N_f are highlighted in different colors.

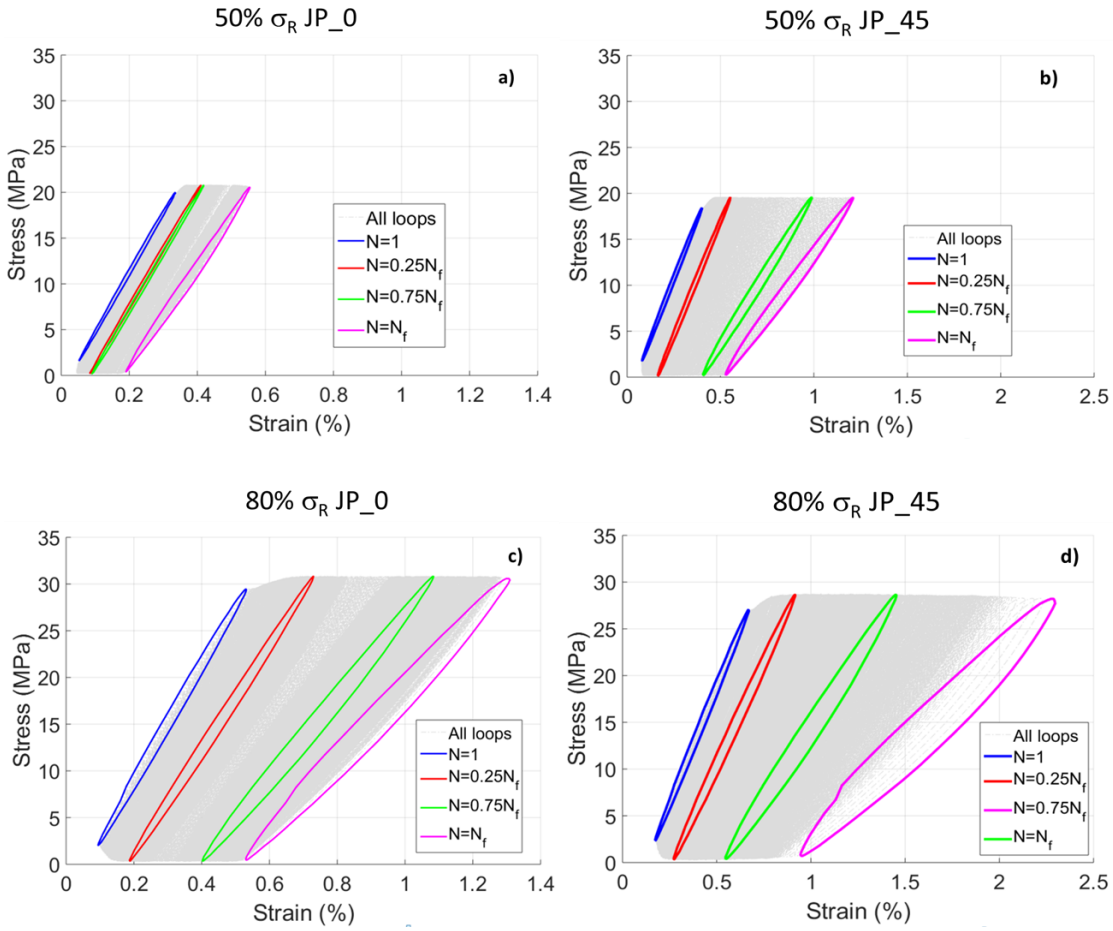

Fig. 4: Hysteresis loops for the fatigue tests for the lower and higher stress levels. a) and c) JP_0, b) and d) JP_45

Stress/strain loops (Fig.4) show that their shape evolves significantly according to the maximum stress level, and the fiber orientation. Each evolution shows a great increase of the residual strain, a progressive decrease of the mean elastic modulus and a progressive increase of internal friction. These evolutions are characterized by a three steps sequence (initial, intermedial and final phases, respectively phases I, II and III), and it can be noticed that for the composite JP_0 tested under low stress levels the evolution of stress/strain loops during the phase II is very low compared to high stress levels and for the composite JP_45. These evolutions are detailed in Fig. 5. Dissipated energy, internal friction and residual strains are also higher for the JP_45 composite than for the JP_0 composite.

Fig.5a and Fig.5b show the evolution of the secant modulus normalized by the measured modulus during the first cycle for each stress level. For the JP_0 laminates, it can be seen that the modulus decrease depends substantially on the stress level. Whatever the stress level, three distinct zones can be observed on the secant modulus evolution. At the beginning of the tests, the secant modulus starts with a strong decrease. This phase is very brief. Then, during the main part of the test (phase II), a steady decrease with a linear trend is observed. The higher the stress level, the more important the slope. It is worth emphasizing that for specimens tested at 50 % of σ_R the secant modulus increases then decreases slightly with some fluctuations during the second phase. Towards the end of the test (phase III), a strong acceleration of the decrease is observed leading to the final failure of samples. For high stress levels, the third phase is less marked because of its brevity (few cycles) comparing to low stress level.

The increase and the fluctuation of the modulus for low stress levels are maybe due to the stiffening effect of the composite samples caused by the reorientation of the microfibrils within jute fibers or a strain induced crystallization of the amorphous cellulose [8,9]. This effect is more pronounced under the low stress levels, because the damage is less extended when compared to high stress levels.

For the JP_45 laminates, the modulus variation does not depend on the stress level. However, the modulus decrease is more significant compared to the JP_0 laminates. Similar results have been observed on flax/epoxy composite [8] showing that the behavior of the off-axis composites is more sensitive to the matrix influence.

The evolution of the maximum and the residual strains during fatigue tests for every layup is presented in Fig. 5c and Fig. 5d. It can be noticed that the strain levels reached during the tests depend strongly on the fibers orientation. Indeed, they are more significant for JP_45 laminates. This is mainly due to the less brittle behavior of these laminates, as indicated by

the static tests [6]. The increase of the stress level tends to increase the strain amounts of the specimen for the two types of composites. Contrary to the maximum stress, the residual one is less sensitive to applied stress level for the two layups. Finally, we note that for the two layups, the evolution of strains occurs in three distinct phases corresponding to those identified for the evolution of the secant elastic modulus. Phases I and III are characterized by a significant increase of deformations.

The evolution of the internal friction for the two layups and for the different stress levels is presented in Fig. 5e and 5f. Results show a good correlation between the evolution of the internal friction with that of the secant modulus and strains for the two orientations. Internal friction is sensitive to development of fiber/matrix debonding due to friction of interfaces created locally. Results show that the evolutions are less pronounced for low stress levels for the JP_0 composite. The comparison of curves of the two orientations indicates that the internal friction is more significant for composites JP_45, especially for low stress levels. This is related to the orientation of the fibers at ± 45 ° that further promotes the development of damage at the interfaces.

The three-phases evolution of the mechanical parameters is characteristic of fatigue behavior of composite materials with synthetic fibers [23-25] or with vegetable fibers [1, 10]. The three-phases of evolution are often linked to different phases of damage within composites.

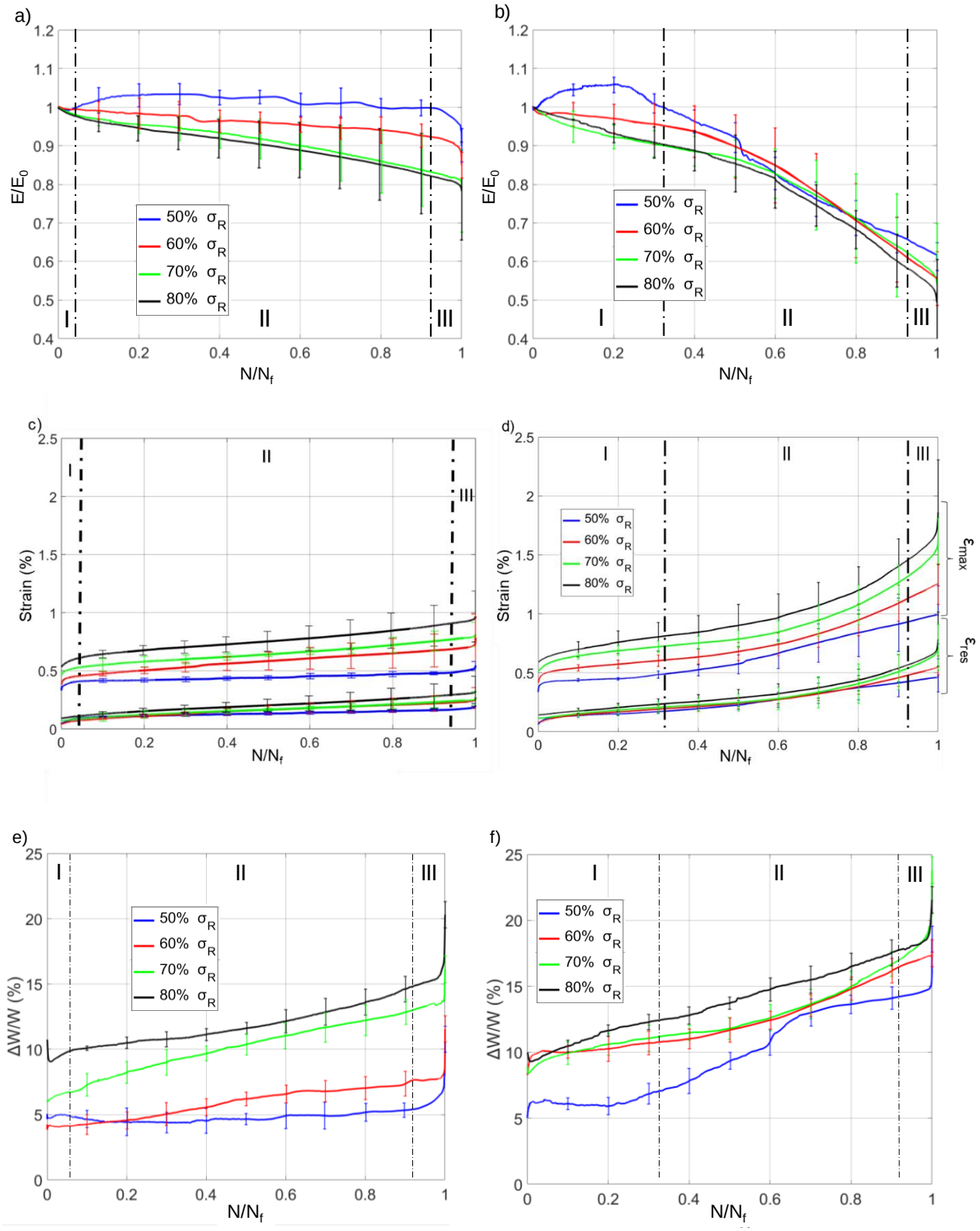

Fig. 5. Evolution of the mechanical parameters versus the normalized number of fatigue cycles: normalized secant modulus (a) JP_0 (b) JP_45, maximum and residual strains (c) JP_0 (d) JP_45, internal friction (e) JP_0 (f) JP_45.

3.3. Damage characterization after failure using X-ray tomography

Fig. 6 presents an example of SEM observations of the fracture surfaces for the two types of specimens. Damage modes observed for fatigue tests were similar to those characterized in static tests. One can observe fiber/matrix debonding (label 1), matrix cracking (label 2) and fiber breakage and pull-out (label 3). However, a difference concerning the matrix cracks density was observed: the crack density appears to be more significant for the specimens loaded in fatigue.

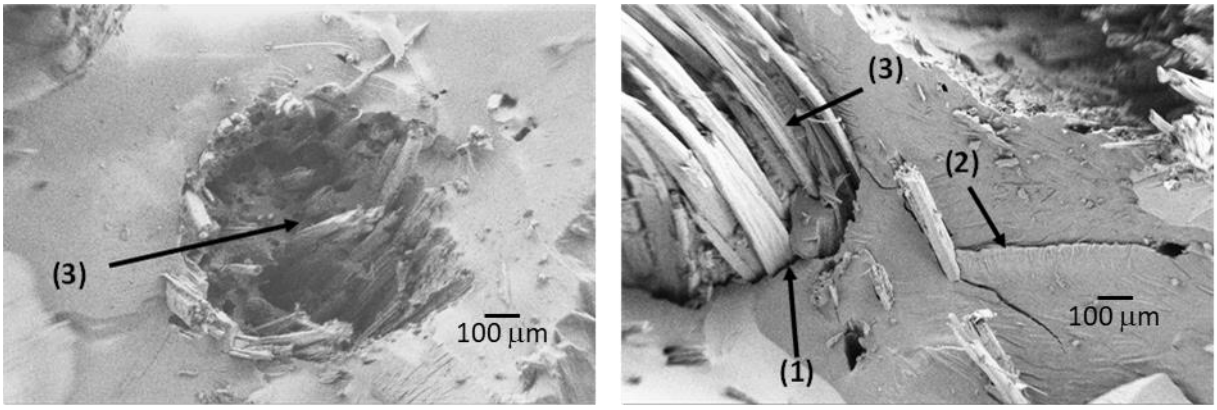

Fig. 6. SEM observations of the fracture surfaces for samples solicited at 80% of σ_R: right JP_0, left JP_45. (1) fiber/matrix debonding, (2) matrix cracking, (3) fiber breakage and pull-out.

To better understand the development of the damage during fatigue tests, a volume inspection of samples extracted from broken specimens (near to the breakage zones) was carried out using X-ray tomography for every stress level and for each type of laminate: JP_0, JP_45. All samples had the same volume and were observed with a resolution of 10 µm/pixel. The interest of this technique is in the investigation of the entire studied volume. Therefore, the analysis of this volume allows quantitative information concerning the development of the damage.

Fig. 7 and 8 present images corresponding to the lower (50%) and the upper (80%) stress levels for the two types of specimens. Contrary to observations obtained for static tests [6], the images show the presence of many matrix cracks (label 2) for samples loaded in fatigue. For both lay-ups no delamination is observed whatever stress level applied. The crack density is related to the stress level. Indeed, the lower stress level, the more important crack

density for the two types of specimens. The matrix cracks appear preferentially perpendicular to the loading axis even for the JP_45 laminates.

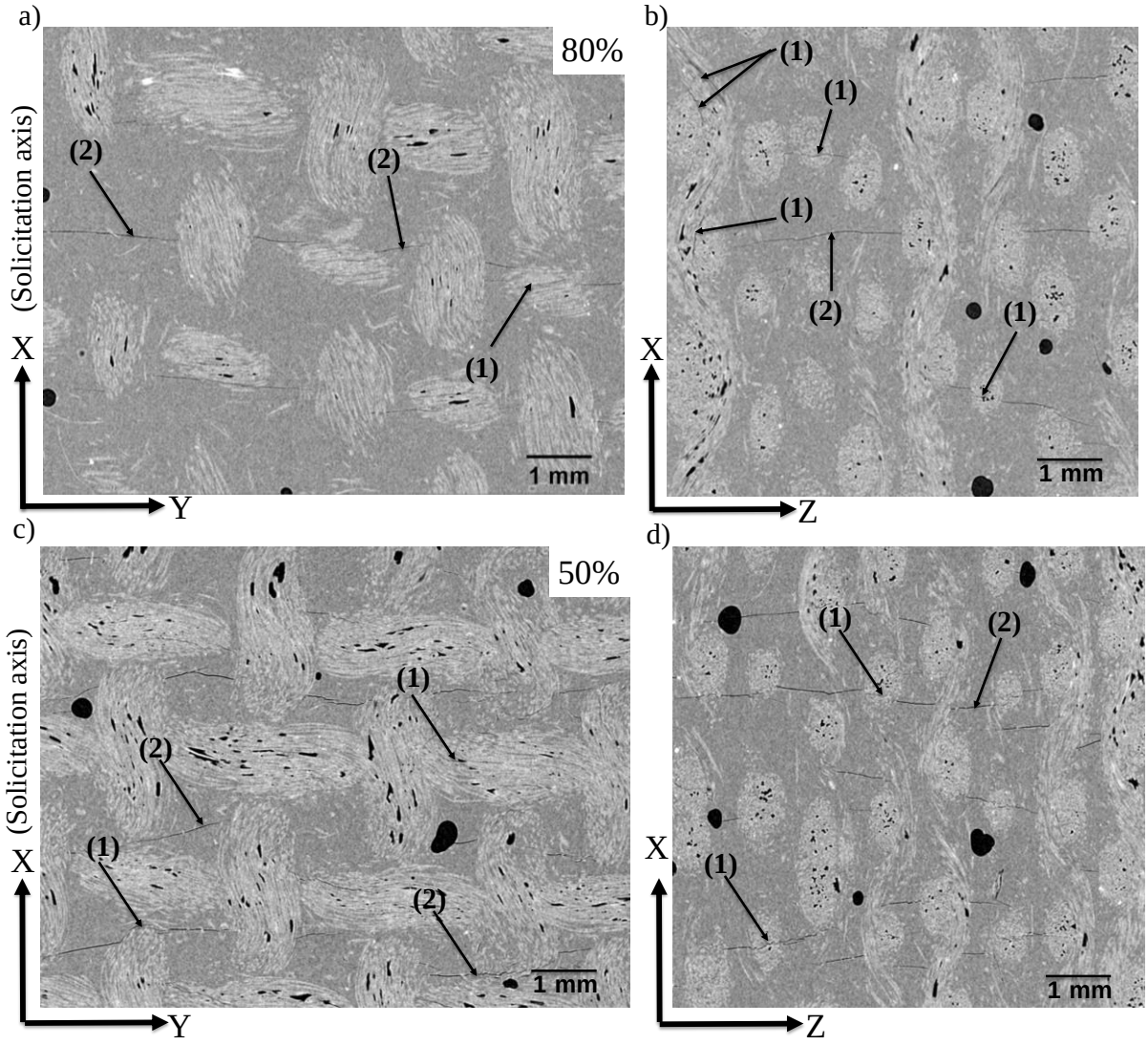

Fig. 7. X-ray tomography images after fatigue fracture for JP_0 specimens: 80% σ_R (a and b), 50% σ_R (c and d), (1) yarn/matrix debonding, and (2) matrix crack, dark points are voids due to residual air bubbles in the resin.

Numerous longitudinal yarns/matrix debondings are observed for JP_0 composites (label 1, Fig. 7). They are more visible for high stress level (80 %) explaining clearly the greater internal friction for these stress levels. Debondings of jute yarns and the matrix are also observed for the JP_45 laminates (label 1). Fig. 7d and Fig. 8d show the corresponding left views of the images obtained at 50% of σ_R for the two layups. For the JP_0 specimen, the cracks propagate in the matrix reach zone and cross the transverse yarns inducing debonding of fibers within the transverse jute yarn.

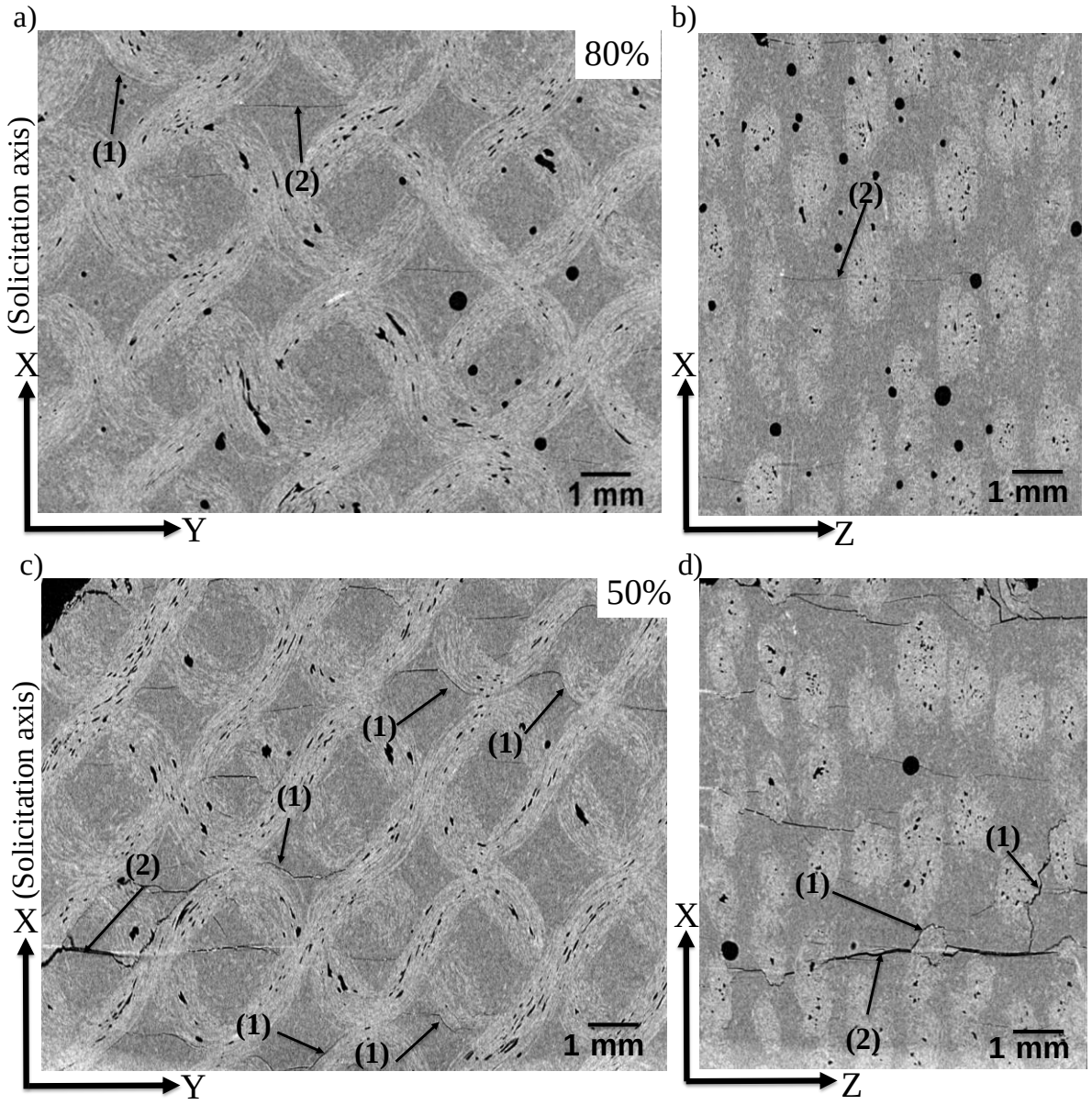

Fig. 8. X-ray tomography images after fatigue fracture for the JP_45 specimens: 80% σ_R (a and b), 50% σ_R (c and d). (1) yarn/matrix debonding and (2) matrix crack, dark points are voids due to residual air bubbles in the resin.

To better illustrate the damage development, the cracks were isolated from a 3D reconstruction of the obtained sections using ImageJ software. The analyses were conducted for the two layups and for each stress level. For every 3D volume, the image treatment is as follows: a grey level threshold has been determined to separate voxels associated with porosities and cracks (which appear in black color in images) from voxels attributed to the material containing matrix and fibers. Then, the cracks were isolated from the rest by applying filters including shape factors in order to remove voids and the intra-yarns

porosities. Fig. 9 shows examples obtained after image treatment of cracks 3D views for the two types of composites (JP_0 and JP_45) samples tested at 50% and 80% σ_R. Due to the 3D connection of the cracks, it was difficult to isolate and count them, and be preferred to calculate a global density from the total volume of cracks.

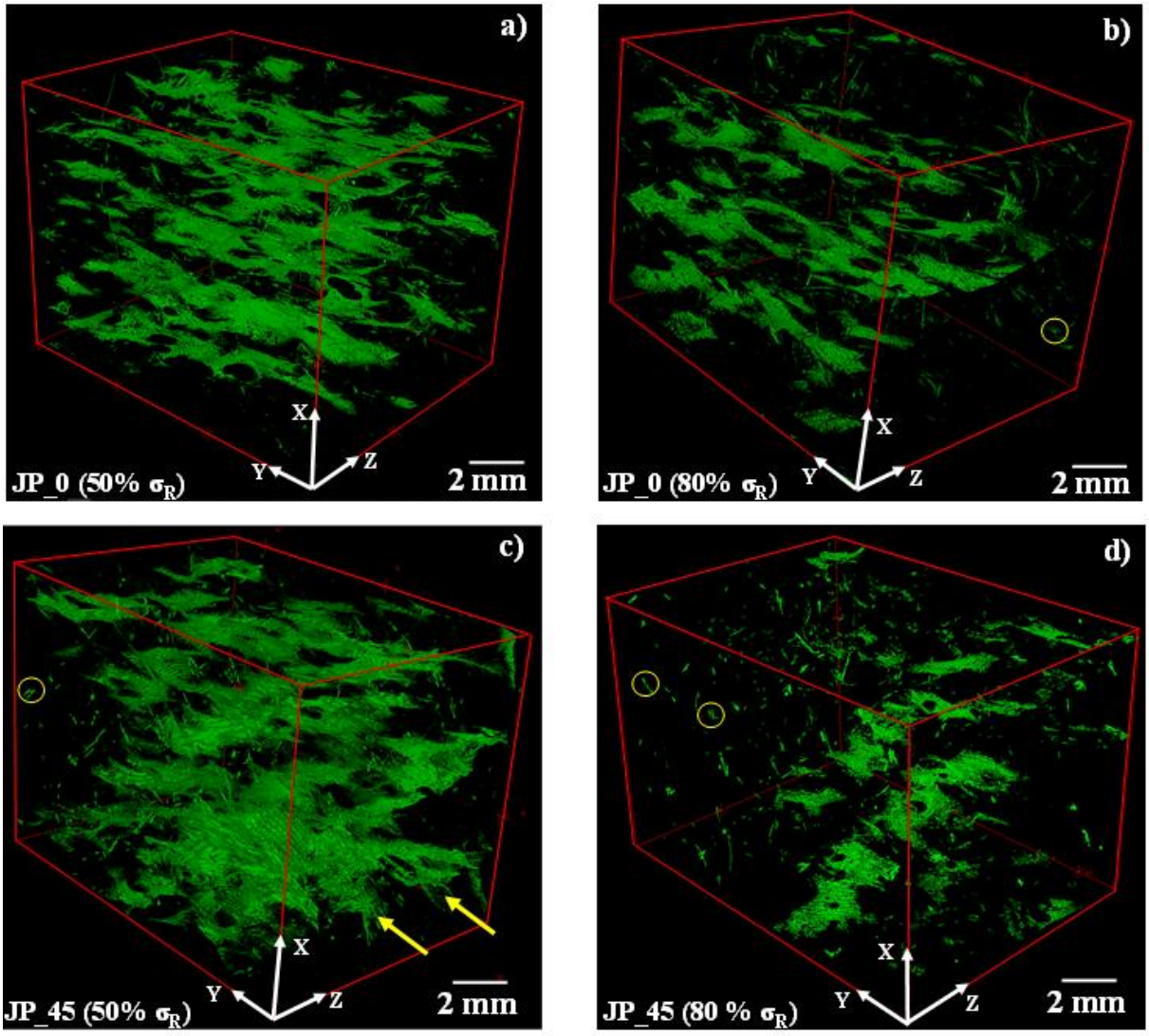

Fig. 9. 3D reconstruction of the crack network for specimens JP_0 (a and b), JP_45 (c and d) after fatigue fracture.

The 3D reconstructions of the damages confirm that the low stress levels present more matrix cracks with a higher density for the samples of the JP_45 composites. For the JP_0 composites, the cracks are mainly located in the matrix rich zone between the plies of the composite and surround the longitudinal jute yarns. Debonding of jute yarns and the matrix can also be observed for the JP_45 laminates (shown with yellow arrows in Fig. 9). They are oriented at 45° from the solicitation axis. Some residues of intra-yarn porosities can be

observed on images (circled in yellow). This is due to the filtering conducted to isolate the cracks.

A quantification of matrix crack density (MCD) was realized for every stress level using ImageJ software. For every 3D representation, the ratio between the volume of damage and the total studied volume of the material was used for comparison between the stress levels. For every stress level, two samples extracted from two different broken specimens were analyzed for the repeatability and the mean value is reported. It is worth to note that the residues of intra-yarn porosity have no influence on the value of the matrix cracks density. Indeed, their volume is very small compared to that of the crack planes.

Table 2 summarizes the obtained results. One can notice that for both types of composites the crack density increases when the fatigue stress level decreases. For the same level of stress, the density is more important for the specimen with higher N_f, which is in accordance with the observations made by X-ray CT. It can be observed that the higher the level of stress, the more the cracks density decreases and approaches the one obtained under monotonic tensile test. When the two composites are compared, it is noticed that JP_45 composites present higher crack density, despite shorter lifetimes. Indeed, the matrix supports more effort for this composite.

Table 2

Matrix crack density calculations for 2 tests at different stress levels and for the two lay-ups.

Stress level	JP_0		JP_45	
	MCD ($\times 10^{-4}$)	N_f	MCD ($\times 10^{-4}$)	N_f
$\sigma = 50\ \% \sigma_R$	33,1	203 059	51,3	148 904
	36,2	547 590	55,7	315 275
$\sigma = 60\ \% \sigma_R$	28,2	30 352	43,9	26 589
	30,2	53 762	47,2	38 230
$\sigma = 70\ \% \sigma_R$	20,2	11 189	25,9	3 221
	15,9	5 696	28,9	5 527
$\sigma = 80\ \% \sigma_R$	12,8	2 116	6,2	995
	13,1	2 548	10,5	1 272
$\sigma = \sigma_R$ (monotonic tensile tests)	6,1	/	8,2	/
	7,2	/	9,7	/

The curve presented in Fig. 10 shows the evolution of the MCD as a function of the number cycles to failure (N_R). For each stress level, the crack density of two samples is presented.

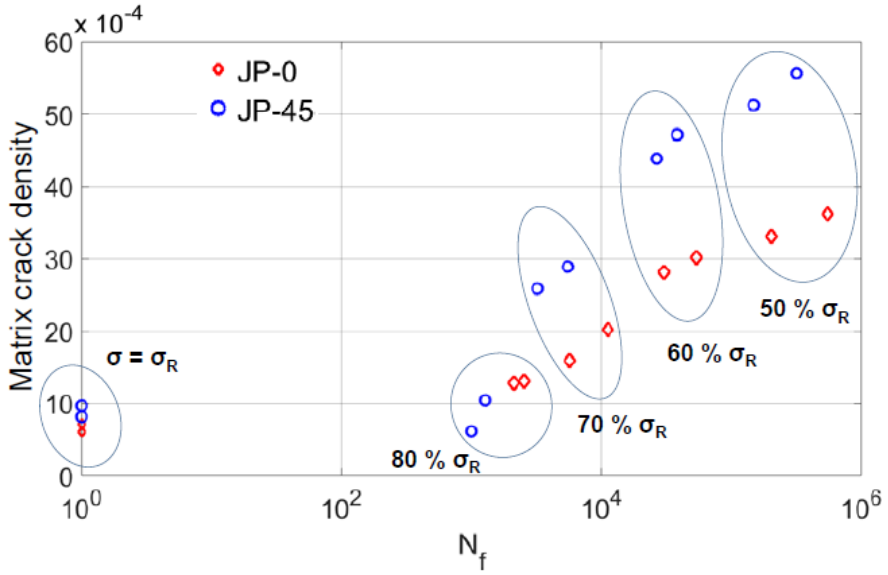

Fig. 10. Evolution of the matrix crack density as a function of the lifetime N_f.

The MCD seems to reach a saturation state as a function of N_f. However, two types of behavior can be distinguished: for low stress levels (50% and 60% σ_R) the density is more important and varies slightly as a function of the number of cycles to failure; on the other hand, for high stress levels, the density is lower and varies significantly with N_f. These two regimes can be linked to two different fatigue behaviors depending on the applied stress.

In order to characterize the evolution of the MCD as a function of the number of cycles, an interrupted fatigue test accompanied by µ-X tomography observations was carried out on JP_45 composite specimen tested at 60% of σ_R. This specific stress level has been chosen to have a good compromise between good damage evolution and intermediate lifetime. The experience consists in testing the specimen for a number of cycles equal to $N_f/6$, then scanning a zone of 12x10 mm (at the middle of the sample) with a µ-tomography. This procedure is repeated until the complete failure of the specimen.

Fig. 11 shows an example of images obtained every $N_f/6$ on the lateral section of the sample (plan (X, Z)). Red arrows indicate fiber/matrix debonding and blue ones indicate matrix cracks.

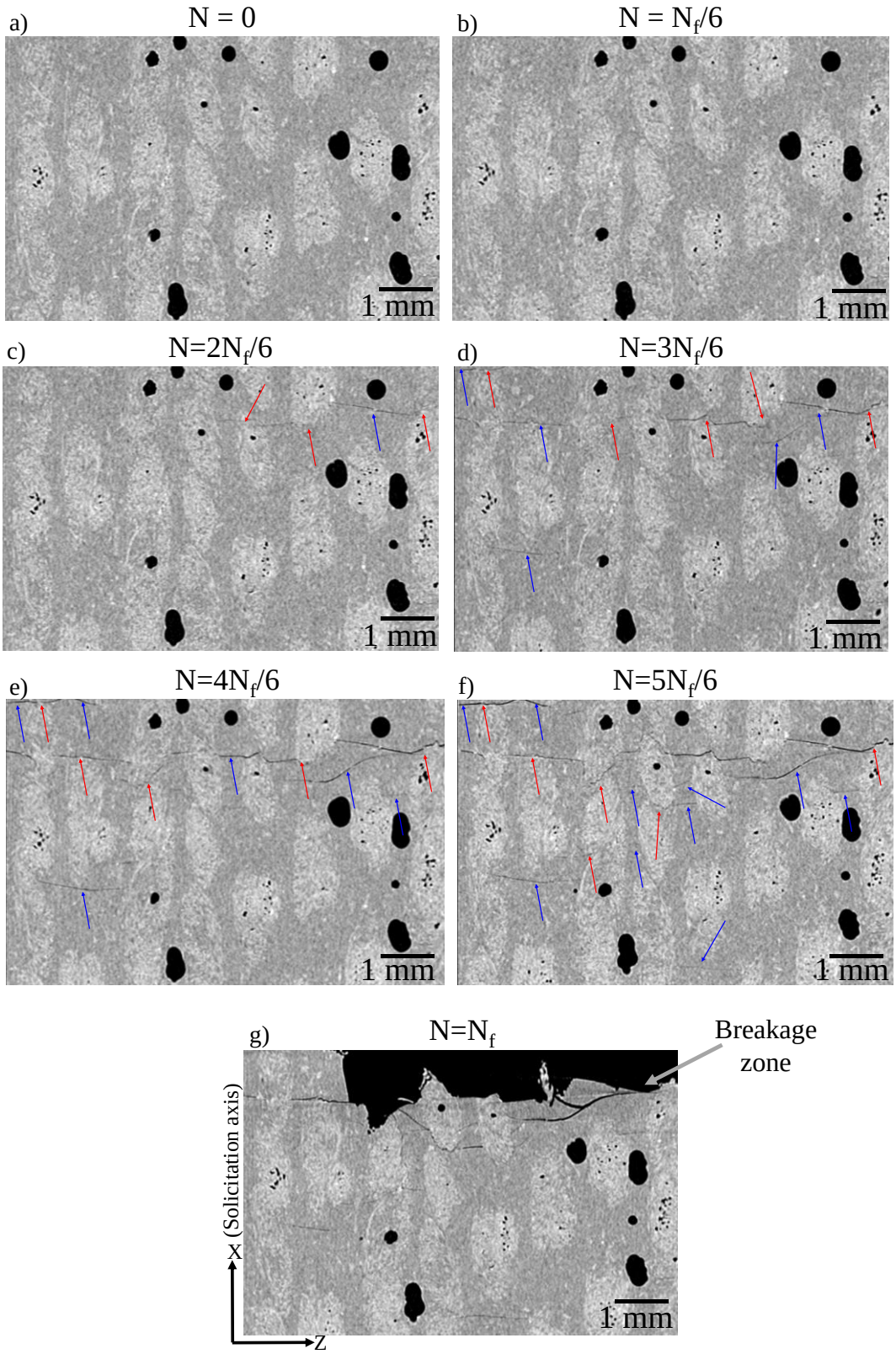

Fig. 11. X-ray tomography micrographs obtained for different numbers of cycles for a JP_45 composite sample tested at 60% of σ_R. Red arrows indicate fiber/matrix debonding and blue ones indicate matrix cracks.

Results indicate that the first matrix cracks appear between $N_f/6$ and $2N_f/6$. It can be seen that these cracks are developed at the edge of the sample, then propagated to the matrix rich zone to merge with fiber matrix debondings. After $N_f/3$, a development of some matrix cracks at the yarn/matrix interfaces can also be observed. The matrix crack density increases with the number of cycles as shown in Fig. 11. It is worth noticing that the final failure of the specimen occurred when the matrix cracks propagated over the whole width of the specimen.

In order to characterize the evolution kinetics of matrix cracks during the fatigue test, a quantification of the MCD was carried out for each number of cycles following the same procedure described above (Fig. 12). The MCD obtained after the failure of the specimen is close to those obtained for the other samples tested at the same stress level (60% of σ_R).

It is worth emphasizing to note that the MCD evolution identified by using tomography fits well with the evolution of the mechanical parameters particularly the evolution of the maximum strain (Fig. 5).

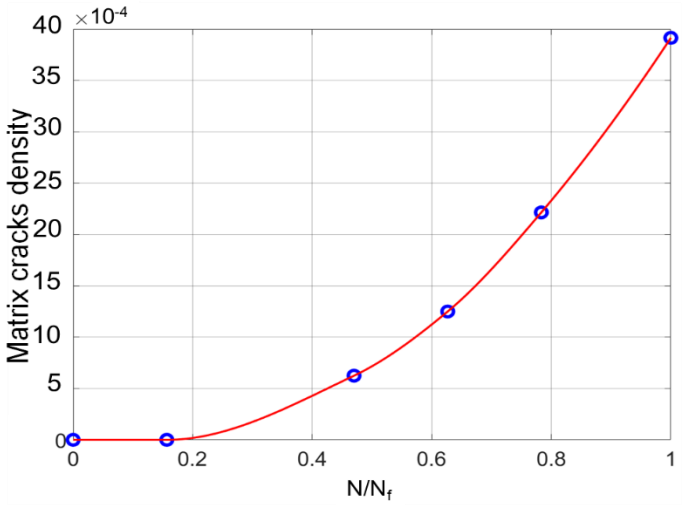

Fig. 12. Evolution of matrix crack density obtained by µ-tomography as a function of N/N_f of the JP_45 specimen tested at 60% of σ_R after several interrupted sequences.

3.4. Acoustic emission results

AE monitoring was conducted continuously during the fatigue tests for all stress levels and for the two studied composite laminates. During fatigue, signals are recorded and descriptors calculated. This allows for example to count them and to sum up their energies as a function of the number of cycles. Fig. 13 presents these evolutions. Cumulated number of AE signals detected and the cumulated AE energy for the two stacking sequences JP_0 and

JP_45 are classical parameters interesting to illustrate the global activity and the scale of the damage mechanisms during a mechanical test in a simple way. The evolutions during fatigue of other descriptors like duration or average frequency have not been determined in the present study, but have been used for the clustering of the signals [22]. As for the mechanical parameters, each curve presents the average values calculated from all the tests and for a given stress level.

It can be observed that for the high stress level, the AE energy is more important compared to the low stress level although a lower number of AE signals is recorded. Moreover, the evolutions of these two AE parameters and the mechanical parameters are in agreement. Indeed, similar evolution in three phases is observed except for the acoustic activity of samples tested at 50% of σ_R. For this stress level, the acoustic activity evolves slightly during the first half of the test then accelerates rapidly until the final failure. These results show that for low stress levels, a large part of the recorded signals is emitted by damage sources with low AE energy sources and with low effects on the mechanical evolution of the specimens. Since the samples tested at 50% of σ_R present a large number of matrix cracks as shown by tomography analyses, these low energy signals might be due to friction phenomena.

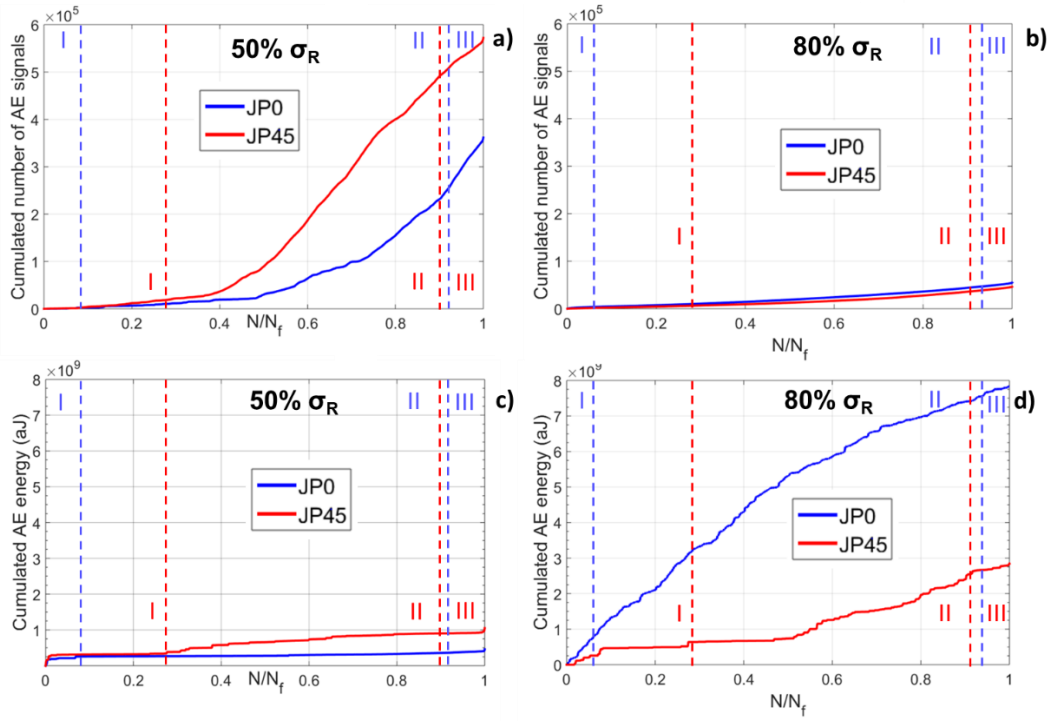

Fig. 13. Evolution of the AE activity (a and b) and the cumulated EA energy (c and d) for two stress levels (50% and 80% of σ_R) as a function of N/N_f.

The AE signals were analyzed by using the supervised classification and the class labelling described in the 2.5 chapter [6]. For this analysis, only the localized signals are considered. It represents between 5 % and 10 % of the total number of the recorded signals (depending on the stress level, the number of signals vary between 6 000 to 60 000). Indeed, the localized signals are inherently emitted by the damage development. So, it is more reliable for the analysis.

Fig. 14 shows the chronology of apparition of the damage mechanisms as a function of the number of cycles for the lower stress level (50% of σ_R) and the higher stress level (80%) for both layups. These AE results are obtained on the same samples which were investigated by X-Ray tomography. For the two composites, a good correlation between the evolutions of the kinetic of damage mechanisms and of the mechanical parameters can be observed.

These results show that the number of AE events related to jute fiber/matrix debonding is preponderant for every stress level and for each composite. Microstructural observations revealed the presence of a large amount of fiber/matrix debondings. It can be noticed that the lower the stress level, the greater the number of matrix cracks. This AE result is consistent with that obtained with X-ray tomography. Fiber breakages are more numerous under high stress levels, being the most severe damage mechanism; that can explain the shorter lifetime of the composites under these high levels of stresses.

When the two composites are compared, one can observe that the number of fiber breakages is more important for JP_0 composites. For high stress levels (Fig. 14), fibers breakages occur continuously during the fatigue test with a strong acceleration towards the composite fracture. On the other hand, for low stress levels, fiber breakages occur mainly during the phase III (just before the failure). It is worth noticing that the evolution of the mechanical parameters evolves slightly during the phase II, although the presence of large number of AE events relating to fiber / matrix debondings and to matrix cracks. For these composites (JP_0), the evolution of the mechanical parameters seems to be mainly related to the evolution kinetics of individual fiber breakage.

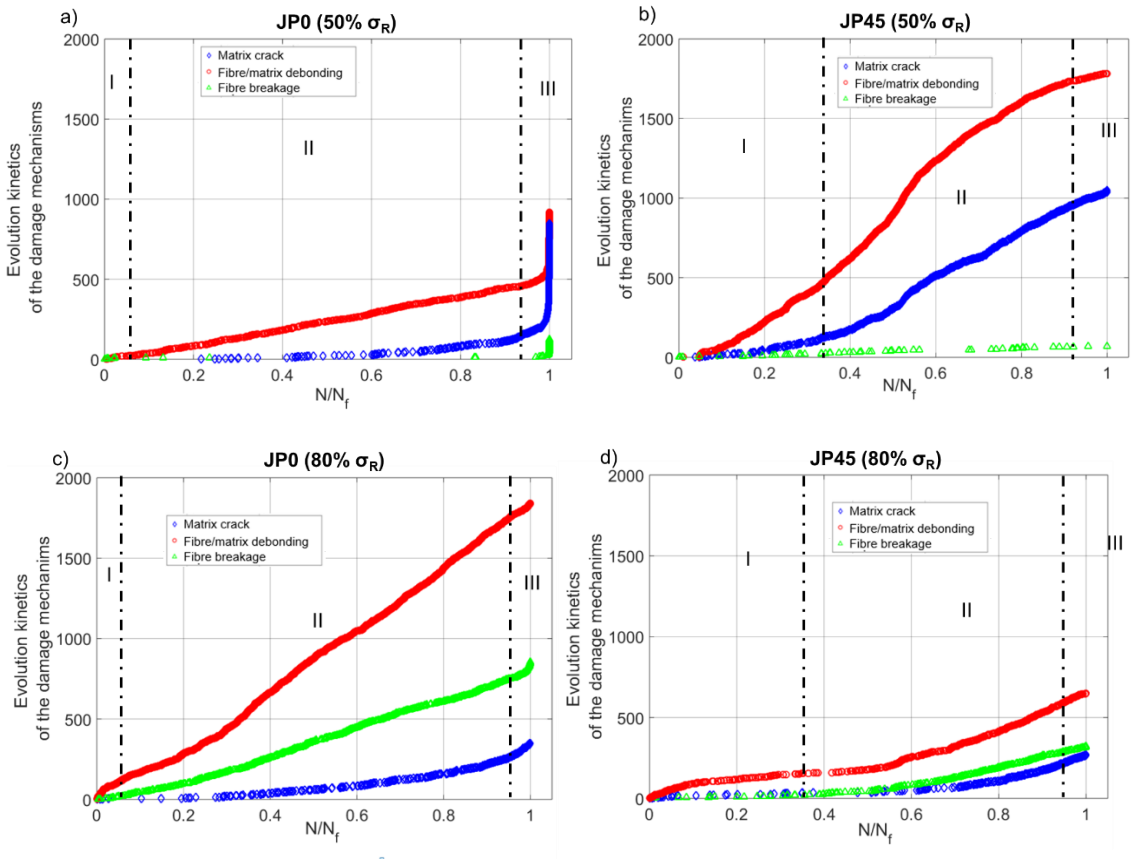

Fig. 14. Evolution kinetics of damage mechanisms during cyclic fatigue as a function of N/N_f for different stress levels and for the two layups: JP_0 (a and c), JP_45 (b and d).

For JP_45 composites, very few fiber breakages are observed under low stress levels. Matrix cracks are more numerous than in JP_0 composites. The kinetics determined from AE are similar to those identified by using X-ray tomography. However, for high stress levels, a large number of fiber breakages is observed. They started during phase I. After that, their number increases significantly with a rapid evolution until the final failure of the samples.

3.5. Scenario of fatigue damage mechanisms

Thanks to the multi-instrumentation and the comparison between mechanical parameters, microstructural observations from microscopy and tomography some scenario may be proposed to determine the main damage mechanisms involved in this original composite, and their evolutions according to the yarns orientations and the applied stress levels. For the two lay-ups the damage scenario depends on the stress level but globally an evolution in three phases is observed, characteristic for the composite materials solicited in cyclic fatigue. These mechanisms are compared and discussed with the mechanisms described in the literature.

3.5.1. NFRP composites in literature

As mentioned in the introduction, in the literature the majority of the papers concerned the mechanical behavior of NFRPs reinforced with flax or hemp fibers [1-4]. The mechanical parameters as stiffness, residual or mean strain follow a 3-stages evolution where the second stage is characterized by a low degradation rate. Fatigue damage modes in NFRPs are similar to those observed during monotonic loading: matrix cracking, fiber-matrix debonding, fiber breakage and pull-out, delamination.

The evolution of damage mechanisms during the three stages are respectively: 1/first stage: transverse matrix cracking and interface damage with some weak fiber breakages, 2/ second stage: development of matrix cracking, significantly along interfaces, and 3/ third stage: macroscopic matrix cracks and interface damage development and yarn failures occurrence. Fiber failures appear early and later during the fatigue life of [0°/90°] composites and are rarely observed for the [+45°/-45°] composites.

Recently, we have studied the static mechanical behavior of jute fiber-reinforced polyester composite and characterized the damage mechanisms using AE and microstructural observations [6]. The damage mechanisms observed were fiber-matrix debonding which is the more significant damage, matrix cracking and fiber breakage.

Here, the analysis of fatigue damage mechanisms is realized by combining different techniques: macroscopic mechanical parameters evolutions, acoustic emission monitoring, microstructural observations, X-ray tomography, allowing the identification of the damage mechanisms and quantify their evolutions during fatigue.

3.5.2. JP_0 composites

The JP_0 composite deforms little and exhibits a lower loss of stiffness than the JP_45 composite. For the low stress levels, the behavior is mainly controlled by matrix cracks (Fig. 15):

- The phase I, for which the mechanical parameters change rapidly, is characterized by the initial damage of the fiber-matrix interface within the transverse yarns and by the ruptures of a few fibers (the weakest). This phase is relatively short.
- The phase II, for which the secant elastic modulus increases, corresponds to the multiplication of fiber/matrix debondings inside the transverse yarns and the development of some matrix cracks. Very few fiber breakages are observed during this

phase. This makes it possible to observe the stiffening of the composite linked to the rearrangement of the yarns.

- The phase III, for which the evolution of the mechanical parameters accelerates rapidly, is characterized by the propagation of transverse matrix cracks, the significant development of fiber/matrix debondings within the longitudinal yarns which will lead to the breakage of the fibers and the total ruin of the specimen.

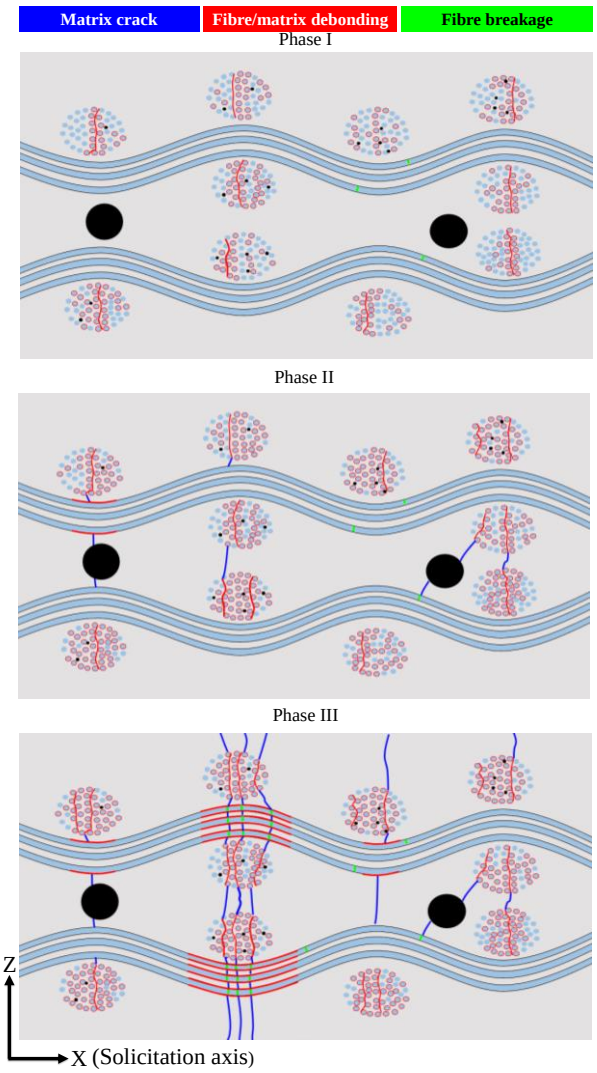

Fig. 15. Fatigue damage scenario of JP_0 composite for low stress levels.

Under high stress levels, the behavior is controlled by the fiber breakages (Fig. 16):

- The very brief phase I is characterized by the breakage of a few fibers and a significant development of fiber/matrix debondings.

- The phase II is characterized by the continuous of fibers breakages resulting from the significant damage of the fiber/matrix interface within the longitudinal fibers and by the development of some matrix cracks.
- When the fiber breaks multiply, the load supported by the matrix becomes greater and will crack leading to the total failure of the specimen. This last phase corresponds to phase III.

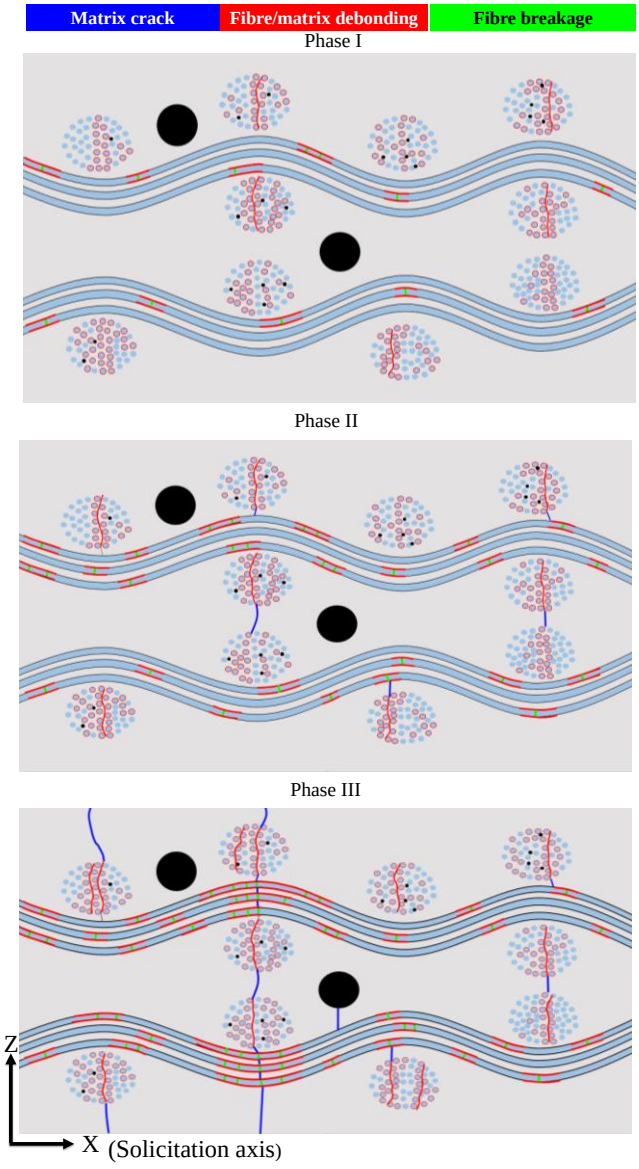

Fig. 16. Fatigue damage scenario of JP_0 composite for high stress levels.

3.5.3. JP_45 composite

JP_45 composites deform strongly during the fatigue test and are characterized by a significant loss of stiffness, except at the beginning under 50% of σ_R where the elastic

modulus increases following the reorientation of the yarns in the direction of the applied stress. The loss of stiffness is due to the orientation of the fibers at ± 45° with respect to the direction of stress. Fiber disorientation also promotes the development of yarn/matrix debondings observed on the evolution of internal friction and matrix damage.

For the low stress levels, the behavior is controlled by the matrix (Fig. 17):

- The phase I is characterized by the development of several yarn/matrix debondings and some matrix cracks.
- The phase II corresponds to the rapid multiplication of yarn/matrix debondings which will promote the development and the propagation of the matrix cracks.
- The phase III, little marked for these stress levels, corresponds to the moment when the matrix cracks propagate over the entire rupture zone of the composite leading to its total ruin. Very few fiber breaks are observed.

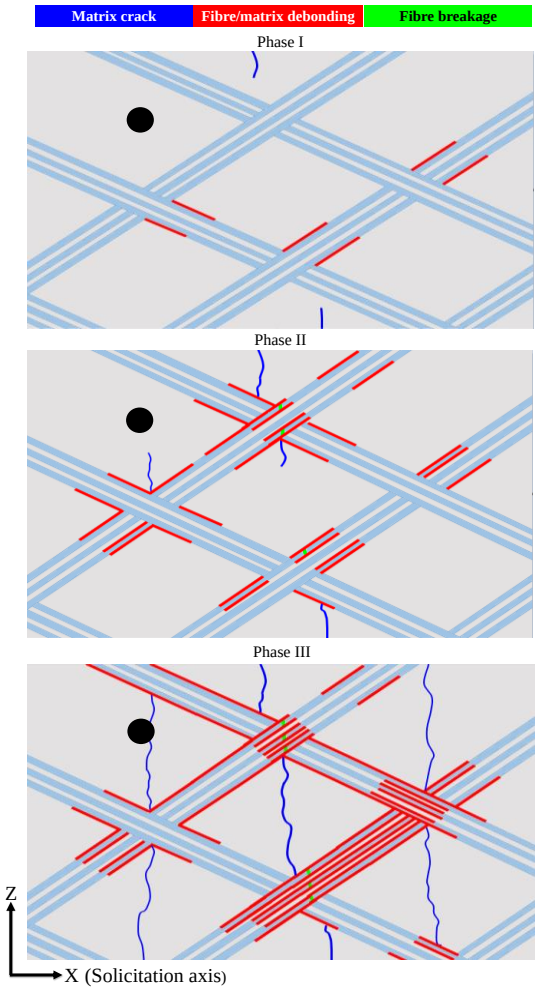

Fig. 17. Fatigue damage scenario of JP_45 composite for the low stress levels.

Under high stress levels, the behavior of composites JP_45 approximates that of composites JP_0. The failure of the composite is controlled by fiber breakages (Fig. 18):

- The phase I is characterized by the rapid development of yarn/matrix debondings.
- The phase II corresponds to the beginning of the development of fiber breaks and to the appearance of some matrix cracks.
- The phase III is characterized by the rapid acceleration of fiber breakages leading to the total ruin of the composite.

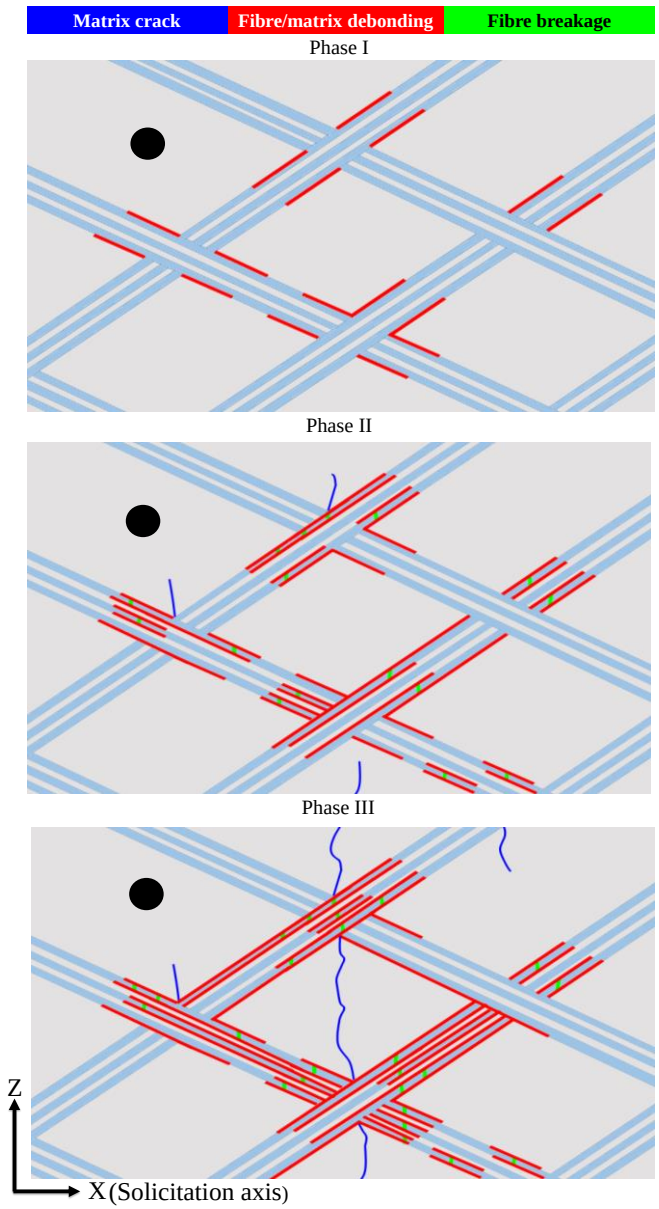

Fig. 18. Fatigue damage scenario of JP_45 composite for the high stress levels.

3.5.4. Comparison between JP_0 and JP_45 composites and NFRP composites of the literature

For both lay-ups there is few fiber breaks under low stress levels, but a more pronounced yarn/matrix progressive debonding along longitudinal yarns, accompanied with micro-cracks initiation and progressive propagation inside the matrix and the transverse yarns. In JP_45 composite debonding occurs mainly close to yarns cross-links and matrix cracks typically propagates in the diagonals of the lozenge matrix cells. Under high stress levels, yarn/matrix debonding is predominant, leading to more numerous fibers and yarns breakages than to propagation of multiple cracks inside the matrix.

Hence for in-use conditions, if an overloading occurs it could propagate yarn/matrix debonding and more increase fibers and yarns breakages, that could reduce the fatigue resistance and the fatigue lifetime of these composites for both yarns orientations (0°/90° and +/-45°).

In comparison with the composites studied in the literature, the scenario described for other composites is similar to the scenario observed here for the JP_0 composite under low stresses, where matrix cracks are predominant. But we have seen here that at higher stresses a new scenario occurs, more controlled by the fiber breakages. This analysis is more accurate than in the literature specifically concerning the effect of the stress. The evolution of the crack density for a given level of stress has been quantified from tomography numerical analyses and acoustic emission analyses using temporal and frequential features, which were consistent.

Concerning the fatigue endurance of the jute/polyester composite studied in this paper, the fatigue limit is lower than 20 MPa for JP_0 composites and lower than 15 MPa for JP_45, whereas the ultimate tensile stress σ_R is 42.9 MPa for JP_0 and 31.1 MPa for JP_45, and during fatigue between these two specific levels of stresses the lifetimes are always lower than 0.5 10^6 cycles for JP_0 and 0.25 10^6 cycles for JP_45. In literature, fatigue properties available for jute, hemp and flax fibers with polyester matrix [12] or epoxy matrix [8, 10] exhibit a fatigue limit higher than 50 MPa, an ultimate tensile strength higher than 100 MPa, and the lifetimes are usually higher than 10^6 or 10^7 cycles. These properties are highly dependent on the fiber volume fraction and less for the type of resin used for the matrices (polyester or epoxy). On the other hand, the fatigue properties might be very sensitive to the

fiber/matrix interfaces, specifically to its strength and its propensity to debond. That could explain why the composite of this study has lower fatigue properties than composites of the literature, and may be improved by surface treatments of the fibers [16]. These treatments may lead to enhance the fiber/matrix interfacial shear strength and therefore limit the fiber and yarn/matrix debonding and its progressive extension during fatigue from yarn cross-links.

4. Conclusion

The present work deals with the fatigue behavior of a woven jute fabrics reinforced polyester resin composites. Two stacking sequences were considered $[0]_8$ and $[+45/-45]_{2S}$. The stress-number of cycles S-N curves were determined. Then, an exhaustive analysis of the fatigue damage is carried out by combining four approaches: the measurement of the mechanical parameters, the microscopic observations by SEM, the X-ray computed tomography, the acoustic emission monitoring.

The measurement of the mechanical parameters revealed the presence of three phases of evolution of the damage. A more marked effect of the stress level on the evolution of the mechanical parameters is observed for the JP_0 composites. An increment in the secant elastic modulus is observed under low stress levels, associated with the stiffening linked to the realignment of the jute yarns.

X-ray tomography revealed the presence of multiple fiber/matrix debondings within the transverse yarns for the composites JP_0 and yarn/matrix debonding for the composites JP_45. The density of matrix cracks is determined, and it is always the more important as the loading level is low, with a higher density for the composites JP_45. Indeed, the matrix takes more effort for this orientation. Two types of behaviors are observed: one for the low stresses and another for the high stress levels.

The AE technique is used to monitor the evolution of damage throughout the fatigue test. Three classes of events are observed corresponding to matrix cracking, fiber/matrix debonding and fiber breakage respectively. The kinetics of evolution of the various damage modes are determined. The results highlighted the greater number of events relating to matrix cracks for the weak stress levels (more marked for the composites JP_45) in agreement with the results of the X-ray tomography. On the other hand, the high stress levels are characterized by a larger number of fiber breakages (more marked for the composites JP_0).

A damage scenario is proposed for each stacking sequence solicited in cyclic fatigue. Under the low stress levels, the behavior is controlled by the matrix and under the high stress levels, the behavior is controlled by the fibers and their debonding. For both orientations, a major

role is played by the yarn cross links, where significant debondings and matrix cracks initiations occur preferentially.

As outlooks for the future, the fatigue behavior can be enhanced by increasing the fiber volume fraction and by increasing the low fiber/matrix interface bonding through appropriate fiber surface treatments.

Declaration of Competing Interest

The authors declare no potential conflicts of interest with respect of the research, authorship, and/or publication of this paper.

Acknowledgements

The authors gratefully thank J. Lachambre for his kind expertise regarding the X-ray tomography analysis , and gratefully acknowledge PROFAS B+ program which allowed this scholarship between INSA Lyon and University Sétif I.

References:

[1] Mahboob Z, El Sawi I, Zdero R, Fawaz Z, Bougherara H. Tensile and compressive damaged response in Flax fiber reinforced epoxy composites. Compos : Part A 2017;92:118-33.

[2] Monti A, El Mahi A, Jendli Z, Guillaumat L. Mechanical behavior and damage mechanisms analysis of a flax-fiber reinforced composite by acoustic emission. Compos : Part A 2016;90:100-10.

[3] De Rosa IM, Santulli C, Sarasini F. Acoustic emission for monitoring the mechanical behavior of natural fiber composites : A literature review. Compos : Part A 2009;40:1456-69.

[4] Scida D, Assarar M ; Poilâne C, Ayad R. Influence of hydrothermal ageing on the damage mechanisms of flax-fiber reinforced epoxy composite. Compos : Part B 2013;48:51-8.

[5] Dobah Y, Bourchak M, Bezazi A, Belaadi A, Scarpa F. Multi-axial mechanical characterization of jute fiber/polyester composite materials. Compos : Part B 2016;90:450-6.

[6] Alia A, Fantozzi G, Godin N, Osmani H, Reynaud P. Mechanical behavior of jute fiber-reinforced polyester composites : Characterization of damage mechanisms using acoustic emission and microstructural observations. J Compos Mater 2019;53:3377-3394.

[7] Sever K, Sarikanat M, Seki Y, Erkan G, Erdogan UH. The Mechanical Properties of γ-Methacryloxypropyltrimethoxy silane-treated Jute/Polyester Composites. J Compos Mater 2010;44:1913-24.

[8] Liang S, Gning PB, Guillaumat L. Properties evaluation of flax/epoxy composites under fatigue loading. Int J Fatigue 2014;63:36-45.

[9] Mahboob Z, Bougherara H. Fatigue of flax-epoxy and other plant fiber composites : Critical review and analysis. Compos : Part A 2018;109:440-62.

[10] de Vasconcellos DS, Touchard F, Chocinski-Arnault L. Tension-tension fatigue behavior of woven hemp fiber reinforced epoxy composite : A multi-instrumented damage analysis. Int J Fatigue 2014;59:159-69.

[11] Shah DU. Damage in biocomposites : Stiffness evolution of aligned plant fiber composites during monotonic and cyclic fatigue loading. Compos : Part A 2016;83:160-68.

[12] Shah DU, Schubel PJ, Clifford MJ, Licence P. Fatigue life evaluation of aligned plant fiber composites through S-N curves and constant-life diagrams. Compos Sci Technol 2013;74:139-49.

[13] Habibi M, Laperrière L, Hassanabadi HM. Effect of moisture absorption and temperature on quasi-satic and fatigue behavior of nonwoven flax epoxy composite. Compos : Part B 2019;166:31-40.

[14] Haggui M, El Mahi A, Jendli Z, Akrout A, Haddar M. Static and fatigue characterization of flax fiber reinforced thermoplastic composites by acoustic emission. Appl Acoustics 2019;147:100-10.

[15] El Sawi I, Fawaz Z, Zitoune R, Bougherara H. An investigation of the damage mechanisms and fatigue life diagrams of flax fiber-reinforced polymer laminates. J Mater Sci 2014;49:2338-46.

[16] Gassan J. A study of fiber and interface parameters affecting the fatigue behavior of natural fiber composites. Compos: Part A 2002;33:369-74.

[17] Asgarinia S, Viriyasuthee C, Phillips S, Dubé M, Baets J, Van Vuure A, Verpoest I, Lessard L. Tension-tension fatigue behavior of woven flax/epoxy composites. J Reinf Plast Compos 2015;34:857-67.

[18] Bensadoun F, Vallons AM, Lessard LB, Verpoest I, Van Vuure AW. Fatigue behavior assessment of flax-epoxy composites. Compos : Part A 2016;82:253-66.

[19] Jeannin T, Gabrion X, Ramasso E, Placet V. About the fatigue endurance of unidirectional flat-epoxy composite laminates. Compos: Part B 2019;165:690-701.

[20] Barbière R, Touchard F, Chocinski-Arnault L, Mellier D. Influence of moisture and drying on fatigue damage mechanisms in a woven hemp/epoxy composite: Acoustic emission and micro-CT analysis. Int J Fatigue 2020;136:105593-606.

[21] D'Amore A, Caprino G, Stupak P, Zhou J, Nicolais L. Effect of Stress Ratio on the Flexural Fatigue Behavior of Continuous Strand Mat Reinforced Plastics. Sci Eng Compos Mater 2011;5:1-8.

[22] Godin N, Reynaud P, Fantozzi G. Acoustic Emission and durability of composite materials. Material Science Series. New York : Wiley-ISTE, 2018.

[23] Morizet N, Godin N, Tang J, Maillet E, Fregonese M, Normand B. Classification of acoustic emission signals using wavelets and Randoms Forests: Application to localized corrosion. Mech Syst Signal Proces 2016;70-71;1026-37.

[24] Reifsnider K, Schulte K, Duke J. Long-term fatigue behavior of composite materials. Long-Term Behav Compos STP 1683;813:136-59.

[25] Vallons K, Zong M, Lomov SV, Verpoest I. Carbon composites based on multi-axial multi-ply stitched preforms – Part 6. Fatigue behavior at low loads: Stiffness degradation and damage development. Compos: Part A 2007;38:1633-45.

[26] Ech-Choudany Y, Scida D, Assarar M, Bellach B, Morain-Nicolier F. Implementation of supervised classification method of acoustic emission signals: damage mechanisms identification of non-hybrid and hybrid flax fiber composites. J Nondestruct Eval 2022;41:1-15.

[27] Farahat M.S., Abdel-Azim A. A.-A., Manar E. A.-R. Modified unsaturated polyester resins synthesized from poly(ethylene terephthalate) waste, 1 Synthesis and curing characteristics. Macromol. Mater. Eng. 2000;283: 1–6